Eddy Formation near the West Coast of Greenland

ANNALISA BRACCO, JOSEPH PEDLOSKY, AND ROBERT S. PICKART

Department of Physical Oceanography, Woods Hole Oceanographic Institution, Woods Hole, Massachusetts

(Manuscript received 25 July 2006, in final form 20 January 2008)

ABSTRACT

This paper extends A. Bracco and J. Pedlosky's investigation of the eddy-formation mechanism in the eastern Labrador Sea by including a more realistic depiction of the boundary current. The quasigeostrophic model consists of a meridional, coastally trapped current with three vertical layers. The current configuration and topographic domain are chosen to match, as closely as possible, the observations of the boundary current and the varying topographic slope along the West Greenland coast. The role played by the bottom-intensified component of the boundary current on the formation of the Labrador Sea Irminger Rings is explored. Consistent with the earlier study, a short, localized bottom-trapped wave is responsible for most of the perturbation energy growth. However, for the instability to occur in the three-layer model, the deepest component of the boundary current must be sufficiently strong, highlighting the importance of the near-bottom flow. The model is able to reproduce important features of the observed vortices in the eastern Labrador Sea, including the polarity, radius, rate of formation, and vertical structure. At the time of formation, the eddies have a surface signature as well as a strong circulation at depth, possibly allowing for the transport of both surface and near-bottom water from the boundary current into the interior basin. This work also supports the idea that changes in the current structure could be responsible for the observed interannual variability in the number of Irminger Rings formed.

1. Introduction

It has been known for some time that an area of high eddy kinetic energy extends from the boundary of the eastern Labrador Sea in the region near 61°–62°N (Heywood et al. 1994; Fig. 1). Recently, it has been shown that this feature is associated with the formation of energetic eddies from the boundary current. The eddies subsequently propagate to the southwest and populate the interior of the Labrador Sea (Prater 2002; Lilly et al. 2003). Various studies have shown that those eddies represent an important flux of heat that helps balance the buoyancy loss through the sea surface during wintertime convection and, during spring and summer, helps to restratify the basin and modify the newly formed Labrador Sea Water found within it (Cuny et al. 2002; Lilly et al. 2003; Eden and Böning 2002; Katsman et al. 2004). A recent investigation of three of those eddies tracked by seagliders hypothesized that they could also be responsible for the annual supply of low-salinity waters to the Labrador Sea interior (Hátún et al. 2007), suggesting that atmospheric fluxes alone (precipitation minus evaporation) are not able to account for the observed seasonality of freshening (Sathiyamoorthy and Moore 2002).

Both cyclones and anticyclones are spawned from the boundary current, but the anticyclones are longer lived and hence are found in greater numbers in the basin. These features are known as Irminger Rings, because of the warm and salty Irminger Water found in their cores, and can extend to great depth (deeper than 2 km; A. Clarke 2002, personal communication). Because of their importance to the formation and evolution of Labrador Sea Water—the major mode water of the North Atlantic—the formation mechanism and structure of the eddies must be determined to understand fully the middepth ventilation of the subpolar gyre.

The processes leading to formation of the Irminger Rings have been addressed in a series of recent modeling studies. Eden and Böning (2002), with a high-resolution ocean general circulation model, and Bracco and Pedlosky (2003, hereafter BP), with an idealized quasigeostrophic channel model, suggested that an in-

Corresponding author address: Annalisa Bracco, School of Earth and Atmospheric Science, Georgia Institute of Technology, Atlanta, GA 30306.
E-mail: abracco@gatech.edu

DOI: 10.1175/2008JPO3669.1

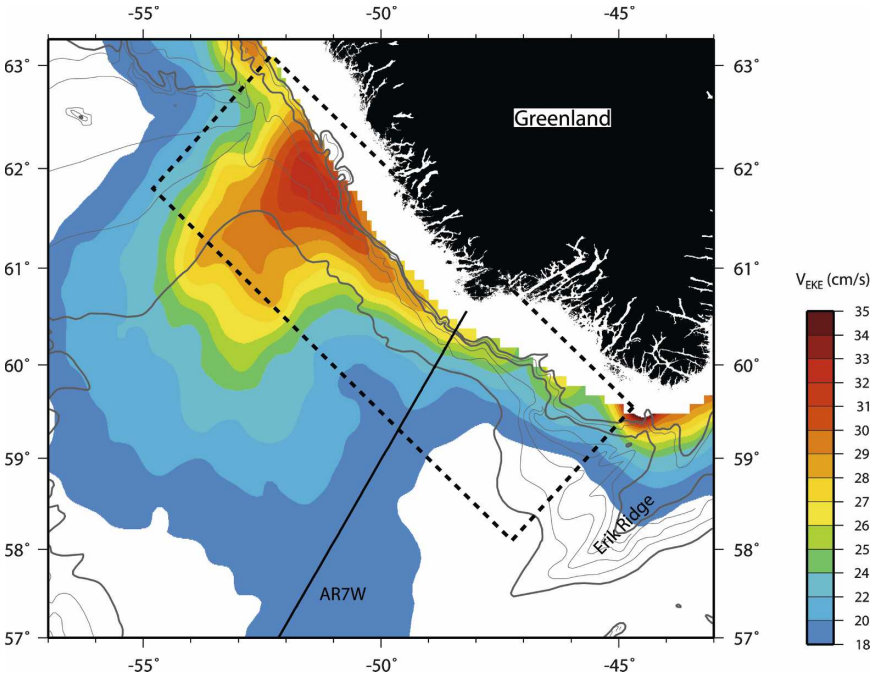

FIG. 1. Distribution of surface eddy speed (color) in the eastern Labrador Sea from Lilly et al. (2003). The dashed box represents the region over which the average bottom slope was computed in Fig. 4a. The location of the World Ocean Circulation Experiment (WOCE) AR7W hydrographic line is marked. The average velocity section of Fig. 2 was computed along the eastern portion of the WOCE AR7W line (see Pickart and Spall 2007). The isobaths are 1000, 2000, and 3000 m (bold contours), and 1500, 2200, 2400, 2600, and 2800 m (light contours).

stability is triggered by the variation in the topography of the continental slope. In particular, the constriction of the isobaths along the West Greenland continental slope, north of Eirik Ridge (Fig. 1), induces an enhancement of the eddy kinetic energy. The mechanism for the instability was mainly barotropic according to Eden and Böning (2002) and baroclinic according to BP. Eden and Böning (2002) found that the strength of the West Greenland Current, influenced by changes either in the wind stress or in the heat flux forcing, was the determining factor for the seasonal changes in eddy kinetic energy of the region. Katsman et al. (2004), using the MIT primitive equation model in an idealized configuration, further explored the sensitivity of the eddy formation to the local bathymetry and the nature of the instability mechanism. They found that the instability process is mixed. In particular, barotropic energy conversion prevails in the upper water column, where heat fluxes in winter strengthen the boundary current, introducing a seasonal signal in the eddy generation, and baroclinic conversion dominates at depth. This last study, however, neglected the vertical structure of the current system, concentrating on the role of heat fluxes.

While the detailed structure of Irminger Rings remains largely unknown due to the paucity of observations in this area, some basic features have been identified. Using mooring data from the central Labrador Sea, along with Ocean Topography Experiment (TOPEX)/Poseidon altimeter data and limited hydrography, Lilly et al. (2003) studied the vortex population in the Labrador Sea over the period 1993–99. They identified and studied 12 Irminger Rings all formed during the period 1997–99. From 1993 to mid-1996 so-called convective lenses were observed, with different characteristics and composition, which likely formed in the interior of the Labrador Sea. The Irminger Rings are warm-core anticyclones with surface-intensified circulation, ranging in radius from 15–30 km, which is significantly larger than the Rossby deformation radius in the Labrador Sea interior (on the order of 10 km). Some of the rings appear to have a "double-core" structure with a second velocity maximum at depth (Lilly et al. 2003). While it is presently unknown how common or robust this feature is, it is clear that the eddies have a deep-reaching signature in both density and circulation.

In the earlier study of BP, a two-layer zonal flow was

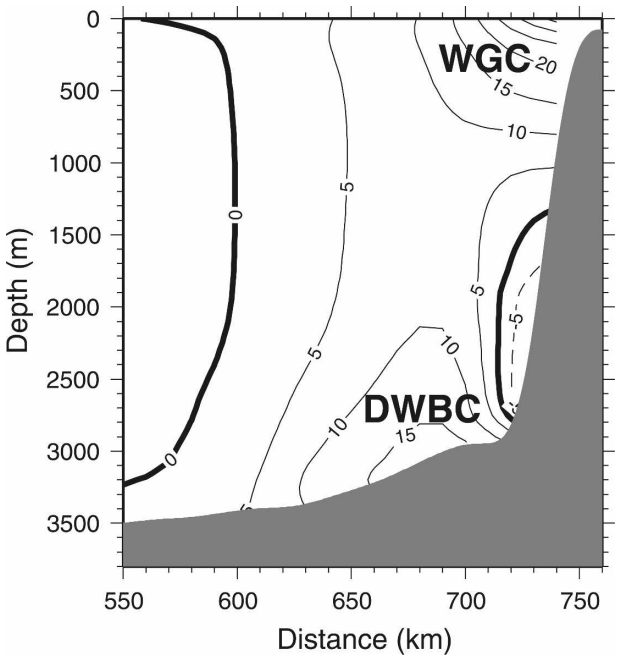

FIG. 2. Average velocity of the boundary current system in the eastern Labrador Sea. Solid contours correspond to poleward flow. WGC denotes West Greenland Current; DWBC denotes deep western boundary current. This is a smoothed version of the velocity field of Pickart and Spall (2007).

considered, to focus on the role of the topography in the generation of the eddies. However, the Labrador Sea boundary current runs NW–SE at about 40° and is more aptly represented as a meridional flow composed of three layers, with the swift West Greenland Current occupying the upper layer, weaker flow at middepth, and the bottom-intensified deep western boundary current at the base of the continental slope (Fig. 2). The goal of the present study is to explore the role of the bottom-intensified flow on the instability mechanism and the structure of the Irminger Rings. To do so we consider a three-layer configuration of a simple quasigeostrophic model with the inclusion of a meridional, coastally confined current system. The topographic slope, background velocity, and lateral scale of the boundary current are chosen to match, as closely as possible, the observed boundary current characteristics along the West Greenland coast. Our focus is on the vertical structure of the vortices at the time of formation, in particular on their signature at depth and on the role that the current structure plays. In this work we do not investigate the restratification processes that may take place in the eddies during spring and summer, once they have filled the Labrador Sea interior. Therefore, an adiabatic model serves our goal without loss of generality. As shown by Katsman et al. (2004), surface heat fluxes are important because they introduce a pronounced seasonal cycle by increasing the temperature contrast between the boundary current and the interior of the Labrador Sea at the end of winter. This contrast strengthens the boundary current, as shown by Spall (2004).

Section 2 contains a brief description of the model used. Results are presented in section 3. In the discussion of section 4 we explore the possibility, proposed by Lilly et al. (2003), that changes in the current system may be responsible for the interannual and decadal variability of the eddy field off of the West Greenland coast.

2. The model

We consider a baroclinic meridional flow confined in an infinitely long channel of width $L^* = 300$ km. The flow is assumed for simplicity to be quasigeostrophic on the beta plane (see, e.g., Pedlosky 1987), and horizontal velocities are independent of depth within each layer. We consider for simplicity three layers of equal depth, $H_1 = H_2 = H_3 = 1000$ m. (The independence of our results on this assumption has been tested by performing numerical experiments with H_3 varying in the range $H_1 \le H_3 \le 1.5H_1$, whereas $H_3 \sim 1.2H_1$ is probably the most relevant to the West Greenland Current system.)

The equations of motion, nondimensionalized as in BP, are

$$\frac{\partial Q_i}{\partial t} + J(\psi_i, Q_i) = \nu\nabla^4\psi_i, \quad i = 1, 2, 3, \tag{1}$$

where ψ_i is the streamfunction in layer I and Q_i is potential vorticity given by

$$Q_1 = \nabla^2\psi_1 - F_1(\psi_1 - \psi_2) + \beta y, \tag{2a}$$

$$Q_2 = \nabla^2\psi_2 - F_2(2\psi_2 - \psi_1 - \psi_3) + \beta y, \tag{2b}$$

$$Q_3 = \nabla^2\psi_3 - F_3(\psi_3 - \psi_2) + \beta y + h(x, y). \tag{2c}$$

Also, ν is the nondimensional coefficient of the horizontal turbulent mixing and J is the Jacobian operator $J(a, b) = \partial_x a\partial_y b - \partial_y a\partial_x b$. The $\nabla^2\psi_i$ terms are relative vorticity contributions. For three layers of equal depths, the interface displacement coefficients F_i are

$$F_1 = F_2 = F_3 = \frac{f_o^2 L_R^2}{g' H} = 1. \tag{3}$$

The internal Rossby deformation radius L_R is used to scale horizontal lengths, while $g' = g\Delta\rho/\rho$ is reduced gravity and f_o is the value of the Coriolis parameter at the central latitude of the domain. In our calculations, we assume $L_R = 12$ km. The parameter $\beta = \beta^* L_R^2/V \sim$

0.016 measures the relative size of the gradient of planetary potential vorticity to the gradient of vorticity associated with vertical shear, with β^* being the dimensional northward gradient of the Coriolis parameter. We take $\beta^* = 1.1 \times 10^{-11}$ s^{-1} m^{-1} and $V \sim 10$ cm s^{-1}. The gradient of the Coriolis parameter is small at this scale and latitude, and its effects are negligible. In the configuration of relevance to the West Greenland Current, similar results are found for $\beta^* = 0$.

The nondimensional bottom relief is $h(x, y) = h^* f_o L_R / v_3^* H_3$, where h^* is the dimensional amplitude of the topography and v_3^* is the characteristic (dimensional) along-shelf velocity in the bottom layer, which contributes to the potential vorticity of the lower layer. Similar to BP, the bottom relief has the form

$$h(x, y) = \gamma(y)(L/2 + x) \quad \text{for} \quad -L/2 \le x \le 0, \tag{4a}$$

$$h(x, y) = 0 \quad \text{for} \quad -L \le x < -L/2, \tag{4b}$$

where γ is a function of the meridional coordinate y, and x varies in the interval $[-L, 0]$.

The streamfunction of the mean flow can be written as

$$\psi_i(x, y, t) = \frac{A_i}{\lambda_i} e^{\lambda_i(x)} + \phi_i(x, y, t) \qquad i = 1, 2, 3, \tag{5}$$

where the first term on the right-hand side is the mean streamfunction ϕ_i, $i = 1, 2, 3$ are the perturbation streamfunctions in each layer; A_i is the maximum values of the velocity associated with the prescribed mean flow; and λ_i^{-1} provides a measure of the width of the boundary current in each layer, set to be $5 \times L_R$ (i.e., 60 km in dimensional units) for all layers for simplicity. The current profile requires the coast to be modeled as a slip boundary. The flow has no inflection points and is therefore barotropically stable in the absence of topographic features.

A schematic of the model domain is given in Fig. 3. The steepness of the continental slope varies in the meridional direction in accordance with the observed bathymetry within the dashed box of Fig. 1. Specifically, the average bottom slope in the Labrador Sea as a function of alongslope distance was computed (Fig. 4a) and used to construct the smoothly varying curve of Fig. 4b. We consider a meridional channel of width $L = L^*/L_R$ in nondimensional units, and we set $\gamma(y)$ to be a positive-definite function following the curve of Fig. 4b, according to

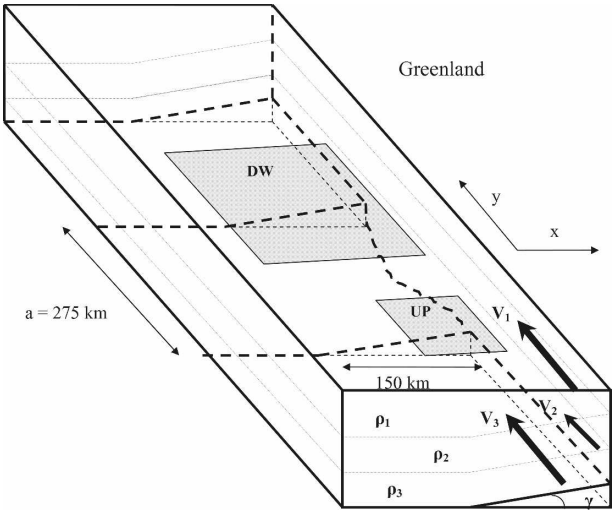

FIG. 3. Schematic of the model geometry. The topography and the current configuration destabilize the flow in the interval denoted by "a." The shading boxes UP and DW indicate the two domains zoomed in Figs. 7 and 8. Here, $x = 0$ along the eastern boundary.

$$\gamma(y) = c - b\left(\tanh\frac{y + a/2}{\sigma'} - \tanh\frac{y - a/2}{\sigma''}\right) \Big/ \left(2\tanh\frac{a/2}{\sigma''}\right). \tag{6}$$

This essentially divides the channel into three areas: an upstream and a downstream region of moderate slope, separated by a region of length a, where the slope is sufficiently small so as to be considered a vertical wall, adjacent to a flat bottom (see Fig. 3). Note in Fig. 4 that the southern transition from a moderate slope to a flat bottom is less abrupt than the northern transition from a flat bottom to a moderate slope ($\sigma' > \sigma''$). These transitions are hereafter referred to as "steps" that bracket the central region a where the bottom is nearly flat. With this choice, the model bathymetry destabilizes the flow in the interval a [see Samelson and Pedlosky (1990) and BP for more details on the instability process].

The average along-shelf velocity of the currents in the three layers, based on the average velocities of the boundary current system shown in Fig. 2, are taken to be $v_1^* \sim 12$ cm s^{-1} for the surface layer, $v_2^* \sim 6$ cm s^{-1} for the middle one, and $v_3^* \sim 10$ cm s^{-1} for the bottom layer. The dependence of the results on the background velocity values is discussed briefly in the following section.

We numerically integrate Eq. (1) and its linearized counterpart constrained by the conditions of no geostrophic velocity normal to the boundary at the longitudinal walls and with meridional periodic boundary

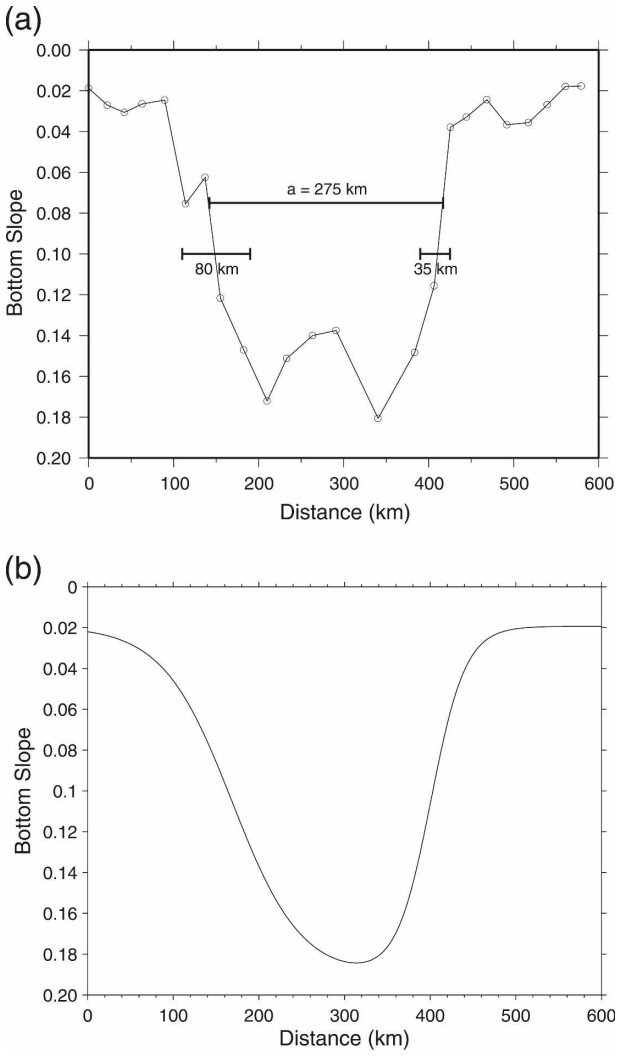

FIG. 4. (a) Average bottom slope progressing northward along the continental slope of West Greenland, computed within the dashed box in Fig. 1. (b) The average bottom-slope profile used to construct the γ function in the model.

conditions. We use a third-order Adams–Bashford integration scheme and a nonaliasing spectral transform method to evaluate the perturbation velocity fields. To simulate the effects of a meridionally infinite domain, a sponge region covers the first 1/8 of the channel. Within this region, a damping with friction coefficient increasing from zero at the border to one at the center is artificially introduced to absorb most of the energy leaving the northern boundary of the periodic domain. This allows us to suppress global modes that may arise in a periodic domain if a wave packet passes repetitively through the same unstable zone. The horizontal resolution of the model is 1.2 km. Such a high resolution is used for ensuring a smooth representation of the topographic step and, more importantly, an accurate representation of the latitudinally confined boundary current. An integration at a spatial resolution of 2.4 km was also performed at a lower Reynolds number with qualitatively analogous results slightly deteriorated by numerically generated noise.

The linear solution allows us to evaluate the nature of the instability (see also BP). Random initial perturbations are allowed to evolve until the most unstable eigenmode emerges. This technique restricts us to the most unstable eigenmode that dominates the evolution after a sufficiently long time. Nonlinear solutions are initialized in two ways: starting from random initial perturbations or by equilibrating linearized solutions with amplitudes normalized to ensure that the perturbations are within the linear regime. Results are independent of the initialization chosen.

It is worth noting that the horizontal potential vorticity gradient changes sign between the first and second layer [$(\partial q_1/\partial x) < 0$, while $(\partial q_2/\partial x) > 0$] and that the system is prone to baroclinic instability everywhere in the channel. Additionally, the proposed basic state of the deep layer with no perturbation is not a steady solution of the equation of motion because, with a nonzero bottom current, there is an interaction of the current with the bottom topography. Thus, in principle, the basic steady flow may also contribute to the evolution of the perturbation field.

To further investigate the nature of the instability, we also integrated the barotropic form of (1), namely,

$$\frac{\partial Q}{\partial t} + J(\psi, Q) = \nu\nabla^4\psi, \tag{7}$$

where $\psi = (A_3/\lambda_3)e^{\lambda_3(x)} + \phi(x, y, t)$ is the barotropic streamfunction and Q is potential vorticity given by

$$Q = \nabla^2\psi + \beta y + h(x, y). \tag{8}$$

3. Results

The analysis of the energy growth and conversion terms in the linearized solution of Eq. (1) shows that the time evolution of the most unstable mode is dominated by a localized baroclinic instability, as in BP, with conversion predominantly from potential to baroclinic kinetic energy. The frequency and growth rate of this mode are the real and imaginary parts, respectively, of the complex eigenvalue $\omega = \omega_R + i\omega_i$, and they can be easily calculated considering that the perturbation kinetic energy of the system is $E_k = Ce^{-i\omega t}$, with C being a constant. The growth rate ω_i has been determined by computing a long-term average of the growth of the perturbation kinetic energy given by $\varepsilon = (1/2)[d(lnE_k)/dt]$. The frequency ω_R, on the other hand, has been evaluated by performing an exact fit to the local time

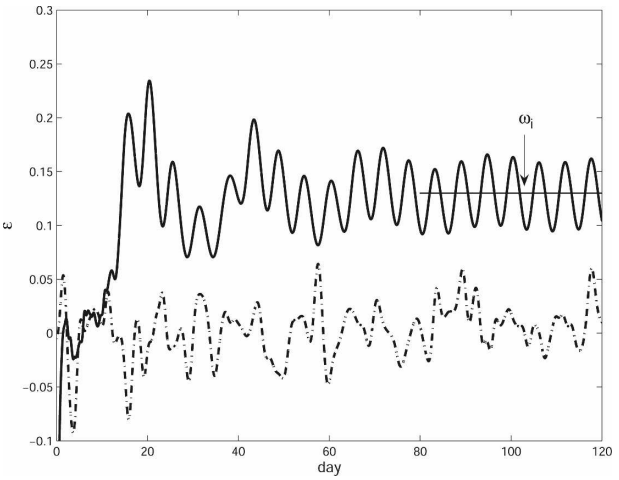

FIG. 5. Time evolution of the kinetic energy growth $\varepsilon = (1/2)[d(lnE_k)/dt]$, in the linear baroclinic (solid line) and barotropic (dashed–dotted) solutions. The growth rate ω_i, i.e., the imaginary part of the complex number such that $E_k = Ce^{-2i\omega t}$, is also shown.

evolution of the energy growth once the form of an eigenmode has been achieved. In nondimensional units, the growth rate for our configuration is 0.13, in agreement with what is found in BP given the width of the boundary current system (Fig. 5). Such a growth rate is much larger than the one associated with the instability induced by the change in sign in the potential vorticity gradient between the first and second layer, making the contribution of the global baroclinic instability negligible (due to the global baroclinic instability ω_i in the three-layer system varies in time by less than 0.01 once the most unstable eigenmode has been achieved). To quantify the contribution of the basic steady flow, we have also integrated Eq. (7) and its linearized form. The growth of the perturbation energy for the barotropic system described by Eq. (7) oscillates around zero and does not display an organized structure (Fig. 5). This allows us to conclude that the kinetic energy production in the three-layer system is dominated by the localized baroclinic instability described in Samelson and Pedlosky (1990) and BP and that the global baroclinic instability and the contribution of the basic steady state are negligible. The nonlinear barotropic solution (not shown) is characterized by a bifurcation of the current with a small portion flowing as a jet along the escarpment at the upstream step and by a fast and continuous generation of small dipoles, with eddies of a radius about 8–10 km formed every 2–3 days, at the downstream step. The barotropic solution, which is not steady, is in agreement with the analysis of Carnevale et al. (1999) for a similar setup, and it is not representative of the observed eddy field along the West Greenland coast. Furthermore, it is far less energetic—over an order of magnitude—than the baroclinic one.

Figure 6 shows snapshots of the potential vorticity disturbances at day 500 of the linear integration of the three-layer system. As in BP, a localized, short bottom-trapped wave is responsible for the majority of the energy growth in the baroclinic system. In the upper and middle layers, the potential vorticity disturbances (Figs. 6b,c) are dominated by a Rossby wave (RW) modified by the shear, similar to the stationary one found in BP and Samelson and Pedlosky (1990), which decays downstream of the escarpment at the northern edge of the unstable interval. In the lower layer (Fig. 6d), the amplitude of the Rossby wave is negligible in the stable region, because the disturbance is in direct contact with the stabilizing bottom slope and decays more rapidly. A narrow oscillating disturbance that attains maximum amplitude near the upstream step distinguishes the evolution of the lower layer, as in BP. The signature of this bottom wavelike (BW) structure is visible in the perturbation potential vorticity field, where two patches of vorticity of opposite sign are recognizable (Fig. 6d). The amplitude of this disturbance reaches its maximum at the upstream step, due to the interaction of the meridional velocities with the meridional gradient of the topography.

The bottom-trapped wave is present whenever

$$\frac{\partial q_3}{\partial x} = (A_3\lambda^2 - A_3 + A_2) + \gamma(y) \tag{9}$$

changes sign from positive to negative. In a three-layer system such as the one chosen, with $\gamma(y)$ being a positive definite function, the contribution to the cross-channel potential vorticity gradient given by the bottom-enhanced boundary current is therefore necessary to the localized instability, and the velocity profile in the second and third layers must be such that $(A_3\lambda^2 - A_3 + A_2)$ is negative but smaller in absolute value than γ. This indeed allows for the required sign change at the upstream corner of the unstable interval. For this form of localized instability to take place, the presence of a sufficiently strong bottom current—sufficiently stronger than the one in the intermediate layer—is essential. We consider this the major result of this analysis, as no previous studies have singled out the deep component of the boundary current as critical to the formation of Irminger Rings.

As in BP, the equilibration of the linear unstable modes produces a dipolar structure in correspondence to the short trapped wave (not shown). The formation process starts in the bottom layer. The two disturbances of opposite sign—cyclonic and anticyclonic—in the

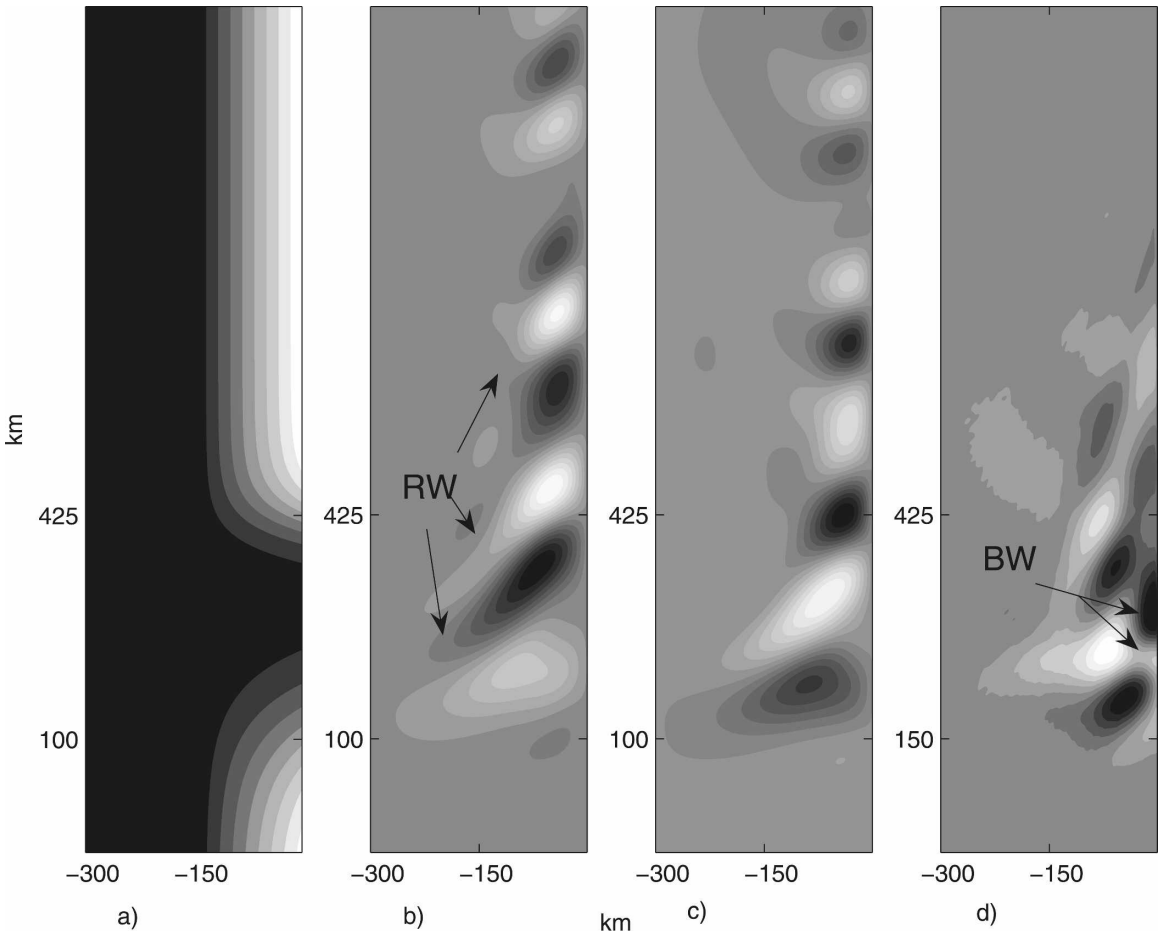

FIG. 6. (a) Bottom slope progressing northward (the x coordinate runs east–west) plotted from the upstream step to the end of one period of the channel (the whole domain of integration extends farther upstream). The region where the flow is supercritical comprises between 150 and 425 km as in Fig. 4. Potential vorticity disturbance at day 500 of integration in the (b) top, (c) intermediate, and (d) bottom layers. RWs dominate the dynamics in the upper two layers, while the BW is visible close to the upstream step in the bottom layer. Bright and dark tones indicate positive and negative potential vorticity, respectively.

deep layer are affected by the image vorticity of opposite sign at the wall (see Carnevale et al. 1997 for a description of the "rebound" process). In particular, once the nonlinear terms are included, the cyclonic perturbation is forced downstream and is deformed by the shear in the current, which is also cyclonic, until it is quickly destroyed (Bracco et al. 1999). (We note that in the first two layers no perturbation is ever found in correspondence with the cyclonic component of the bottom-trapped wave.) This happens in less than a day in our integrations, leaving behind an isolated anticyclonic perturbation.

Figures 7 and 8 show two stages in the evolution of such an anticyclone. Figure 7 shows the feature 2 days after its generation at the upstream step (simulation day 149), and Fig. 8 shows the vortex after it has detached from the boundary at the downstream step (simulation day 160). We first describe the early stage. During the first couple of days after formation, the perturbation strengthens and moves slightly upstream, against the mean current, as an isolated eddy under the influence of its image, which has the opposite sign of vorticity. It takes approximately 1 (3) more day(s) for the amplitude of the anticyclonic potential vorticity perturbation in the intermediate (surface) layer to reach its minimum. Once the anticyclonic eddy is fully formed, it starts moving downstream, carried by the mean current along the wall and over the flat bottom. While doing so, the negative potential vorticity perturbation further intensifies at the surface, extracting kinetic energy from the mean flow and masking the baroclinic origin of the instability. Once the anticyclone reaches the downstream topographic step, it climbs the step and enters into the stable interval. In the stable region, the slope slowly affects the location of the anticyclone and the core of the vortex shifts westward,

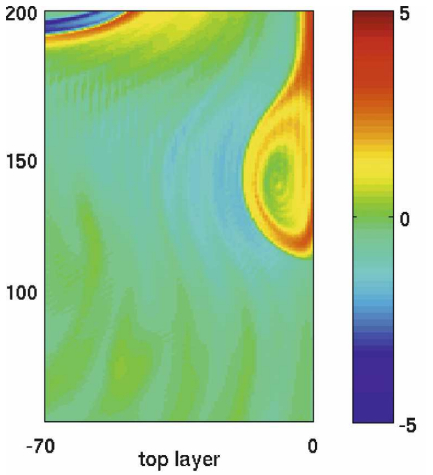

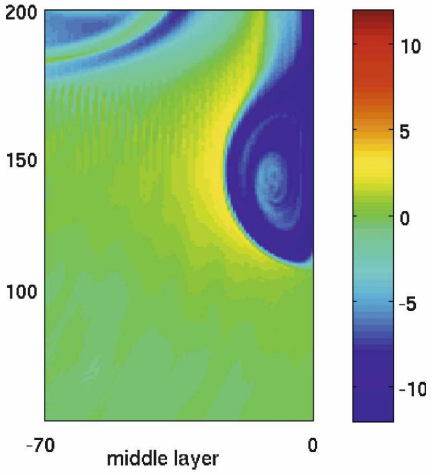

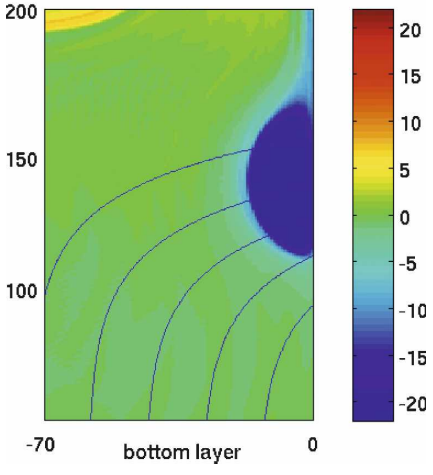

FIG. 7. Enlarged view of the potential vorticity disturbance in the upper, middle, and lower layers with the isolines of the bathymetry overlaid in box UP in the schematic of Fig. 3, which corresponds to the interval 50–200 km in Fig. 4. The wall corresponding to the model equivalent of Greenland is on the right (at $x = 0$) of each panel. The figure shows the formation of an anticyclone at the upstream step. Units are km for both axes.

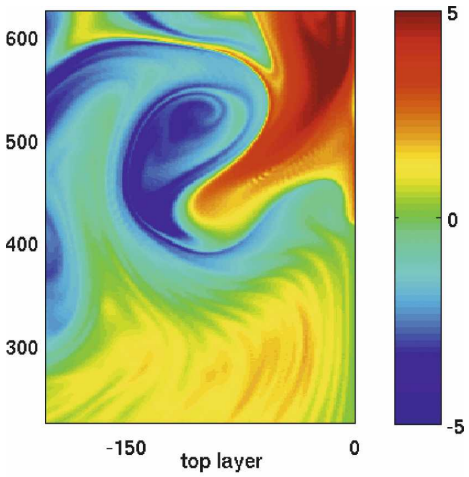

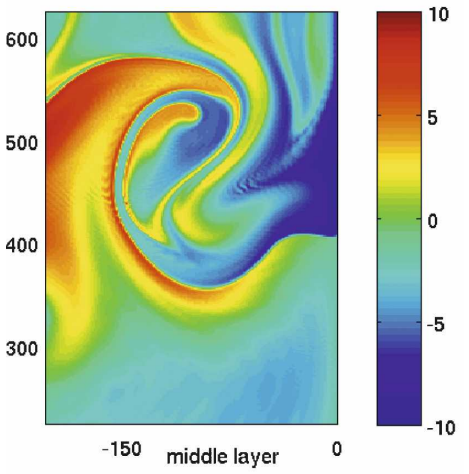

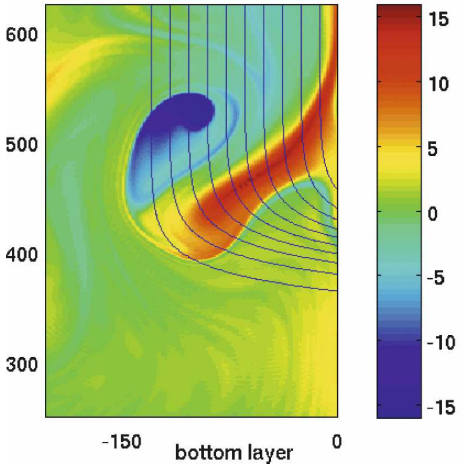

FIG. 8. Enlarged view of the potential vorticity disturbance in the upper, middle, and lower layers with the isolines of the bathymetry overlaid in box DW in the schematic of Fig. 3, which occupies the interval 290–650 km in Fig. 4. Note that the downstream box is about 4 times larger than the upstream box. The wall corresponding to the model equivalent of Greenland is on the right (at $x = 0$) of each panel. This anticyclone formed at the upstream topographic step approximately 10 days earlier (shown in Fig. 7) and is now detaching from the boundary and is forming a dipole. Units are km for both axes.

toward deeper water. In the second stage, roughly 10–12 days after its formation at the upstream step, the anticyclone detaches completely from the boundary at the downstream edge of the unstable interval and moves into the interior of the channel. Indeed, by conservation of potential vorticity, isolated anticyclones over a slope move toward deeper water (e.g., McWilliams and Flierl 1979; Carnevale et al. 1988; Whitehead et al. 1990; Carnevale et al. 1991; Dewar and Gailliard 1994; LaCasce 1998; Jacob et al. 2002). As part of this detachment process, a new cyclone can form, but it is generally weaker than the anticyclone and contains water from the coastal boundary current at the location of the detachment (see Fig. 8). This process is repeated over and over, and the energy growth is fully equilibrated (i.e., a statistical quasi equilibrium is reached) after about 100 days whenever a normalized linear solution is used as the initial condition.

The size of the eddies at the time of formation at the upstream step is determined by the sharpness of the step, as already found in BP with a detailed parameter exploration. The diameter of the anticyclones is roughly half of the step extension, that is, about 35 km (Fig. 4a), in agreement with altimetry data (Lilly et al. 2003). The anticyclonic vortices in the three layers are aligned, with the upper-layer core larger in radius than the bottom layer. This may result from the stabilizing effect of the bottom slope over the edges of the vortices in the lower layer. The rate of formation of new anticyclones is approximately every ~6–7 days. Only about 35% of the eddies formed at the upstream step reach the interior of the basin; the others are reabsorbed into the boundary current or merge with other anticyclones before reaching the downstream step.

Performing a sensitivity study, we have found that reducing the difference in the boundary current velocity between the intermediate and bottom layers to one-half or less of what is presented above alters the stability properties of the flow, causing the vortices that form at the topographic step to be more unstable and not allowing the alignment of the cores in the top and bottom layers. Whenever this is the case, the vortices do not survive long enough to penetrate into the interior of the model domain.

A word of caution is necessary regarding the realism of the model domain in this study relative to two major aspects. First, the geometry of the basin is a crude approximation of the eastern side of the Labrador Sea. We indeed concentrated on representing the observed bathymetry in the region where the flow is locally supercritical (interval "a") and we used a simplified representation of the region included in the dashed box in Fig. 1. Outside such a region, the differences between the model (an infinitely long channel with a stabilizing bottom slope) and the actual bathymetry are significant. In particular, we neglect the northwestward veering of the isobaths at the downstream edge of the interval of instability. Katsman et al. (2004), however, have shown, with a sensitivity study using the MIT general circulation model, that the constriction considered in this work—in particular its upstream step and not the orientation of the topography downstream—is responsible for the vortex formation. The upstream generation of the Irminger Rings is suggested also by a recent analysis of gridded satellite altimetric data performed for the period August 2001–December 2006 (H. Furey and A. Bower 2007, personal communication) and by the eddy-resolving numerical experiments by Czeschel (2005). The downstream veering of the isobaths, however, forces the deep branch of the boundary current offshore, which may help intensify and carry the eddies into the interior of the basin. Second, Irminger Rings in the Labrador Sea display both surface intensification and a seasonal cycle, which are believed to be related to the strengthening of surface heat fluxes during the winter season and to the consequent acceleration of the surface current (Katsman et al. 2004). Our model does not attempt to capture seasonality. However, not surprisingly, the inclusion of a thermal damping between the surface and the intermediate layer induces (in a calculation not shown here) a "barotropization" of the upper two layers and therefore an intensification of the upper-layer disturbances, in the direction of the observed vortex population structure.

The mechanism of formation studied in this work is a compound process involving eddy generation by localized baroclinic instability at the upstream edge of the unstable interval, followed by a northward displacement of anticyclonic vortices along the western wall of the domain, and finally by detachment of single anticyclones or dipoles at the downstream step. This mechanism is able to explain the energy-transfer terms and the distribution of eddy kinetic energy along the coast, within the interval "a," in correspondence to Eden and Böning's (2002) high-resolution ocean general circulation model solutions (see their Fig. 12) and Katsman et al.'s (2004) idealized experiments. It also explains the maximum of eddy kinetic energy found around 61°–62° in TOPEX/Poseidon altimetry data (see Fig. 3 of Prater 2002) as well as the observed radius of the Irminger Rings of approximately 35 km (Lilly et al. 2003). We believe, therefore, that despite the simplifications of our model, the mechanism of vortex formation discussed in this paper is of relevance to the Labrador Sea.

4. Discussion and conclusions

This work describes the dynamics of a quasigeostrophic three-layer meridional current in a north–south channel over variable topography on the beta plane, meant to represent the eastern boundary of the Labrador Sea. The topography slopes uniformly westward in the east–west direction and is a smoothly varying function of the meridional coordinate. It is found that the bottom slope controls the local supercriticality of the flow and is configured to destabilize it in a central interval of limited meridional extent.

Despite the obvious simplifications, the model is able, with realistic choice of the current scales, to reproduce important features of the observed vortex population shed near the western coast of Greenland. This includes vortex polarity and radius (Lilly et al. 2003; Prater 2002), rate of formation as inferred from observations (Lilly et al. 2003; H. Furey and A. Bower 2007, personal communication) and from more sophisticated models (Eden and Böning 2002; Katsman et al. 2004), and observations of the water-column structure of the rings (Lilly et al. 2003; A. Clarke 2002, personal communication). The generation mechanism of stable coherent vortices in our model results from the equilibration of the most unstable mode associated with local baroclinic instability induced by the variable topography (see also Samelson and Pedlosky 1990; BP). As shown in BP, the bottom-trapped disturbance is responsible for the vortex formation and grows to balance the ambient gradient of potential vorticity with time variations of relative vorticity. Subsequently, the initial dipolar structure rebounds from the slip wall and the cyclonic perturbation is quickly destroyed. Only the anticyclonic component survives in the background cyclonic current system, and it penetrates downstream. Once it reaches the downstream topographic step, the eddy enters the basin as a single vortex or as a member of a new dipole, extracting the cyclonic component from the boundary current at the location of the detachment. The net result is an eddy-driven flux of water from the boundary current into the interior of the Labrador Sea, which impacts the entire water column.

Irminger Rings have been observed in abundance since 1997, while a different population of vortices filled the Labrador Sea during the four previous years (the so-called convective lenses). The formation of Irminger Rings is also associated with a stronger annual cycle in the eddy kinetic energy field along the West Greenland coast as compared to the previous period (Brandt et al. 2004). A definitive explanation for this sudden appearance of Irminger Rings is still lacking, but it has been sought in the interannual variability of the (surface intensified) West Greenland Current. While sea surface temperatures along the West Greenland coast were anomalously low in 1997, suggesting a high inflow of polar water, over the following 3 yr they were anomalously high (Buch et al. 2004). Also, surface winds in the same region do not show a clear trend or change during the 1993–2000 period (although it should be noted that the reliability and time resolution of both atmospheric and surface oceanic fields obtained through satellite measurements are limited because of persistent cloud coverage). Hence, it is not obvious how interannual changes in the upper-layer flow are related to changes in eddy formation. Interannual variability in both the surface heat fluxes and the wind stress field, recently suggested to cause the variability of the Deep Labrador Current during the last decade (Dengler et al. 2006), could possibly explain the observed changes in the eddy field off the west coast of Greenland, but this hypothesis is difficult to test using the available data.

Our model suggests that the deep part of the boundary current may play a fundamental role in the interannual variability of eddy formation in the Labrador Sea, a hypothesis supported by the laboratory experiments of Wolfe and Cenedese (2006). The eddies formed in our simple quasigeostrophic model are particularly stable and extend throughout in the water column at the time of formation. Their existence, stability, and vertical profiles are directly linked to the presence of flow in the deep layer sufficiently stronger than the current at middepth and having an intensity roughly the same as the upper-layer current. While stressing that diabatic effects will further contribute to the stability of the upper part of the eddies, possibly reducing the sensitivity of the eddy evolution to the subsurface currents, our work suggests that changes in the production rate and structure of the eddies formed in this region could be associated with variations of the deep western boundary current. This supports the idea that the variability in the overall subpolar gyre transport and circulation, as documented in Hátún et al. (2005), for example, and not only of its surface expression, may impact the generation of Irminger Rings. Further work will test the hypothesis that the variability of the subpolar gyre may modulate the formation of Irminger Rings with a circulation model configured to include the subpolar gyre and the Labrador Sea region.

Acknowledgments. We are grateful to Amy Bower, Fiamma Straneo, and Jonathan Lilly for useful discussions during the preparation of this manuscript. Many thanks to Heather Furley and Amy Bower for kindly sharing the results of their recent analysis on gridded altimetric data. The authors wish to acknowledge the

valuable comments of two reviewers, who helped to improve the clarity of this work. AB is supported by WHOI unrestricted funds, JP by the National Science Foundation OCE 85108600, and RP by 0450658.

REFERENCES

Bracco, A., and J. Pedlosky, 2003: Vortex generation by topography in locally unstable baroclinic flows. *J. Phys. Oceanogr.,* **33,** 207–219.

——, A. Provenzale, E. A. Spiegel, and P. A. Jecko, 1999: Spotted disks. *Theory of Black Hole Accretion Disks,* M. Abramowicz, G. Björnsson, and J. Pringle, Eds., Cambridge University Press, 293 pp.

Brandt, P., F. A. Schott, A. Funk, and C. S. Martins, 2004: Seasonal to interannual variability of the eddy field in the Labrador Sea from satellite altimetry. *J. Geophys. Res.,* **109,** C02028, doi:10.1029/2002JC001551.

Buch, E., S. A. Pedersen, and M. H. Ribergaard, 2004: Ecosystem variability in West Greenland waters. *J. Northwest Atlantic Fish. Sci.,* **34,** 13–28.

Carnevale, G. F., G. K. Vallis, R. Purini, and M. Briscolini, 1988: Propagation of barotropic modons over topography. *Geophys. Astrophys. Fluid Dyn.,* **41,** 45–101.

——, R. C. Kloosterziel, and G. J. F. van Heijst, 1991: Propagation of barotropic vortices over topography in a rotating tank. *J. Fluid Mech.,* **233,** 119–139.

——, O. U. Velasco Fuentes, and P. Orlandi, 1997: Inviscid dipole-vortex rebound from a wall or coast. *J. Fluid Mech.,* **351,** 75–103.

——, S. G. Llewellyn Smith, F. Crisciani, R. Purini, and R. Serravalle, 1999: Bifurcation of a coastal current at an escarpment. *J. Phys. Oceanogr.,* **29,** 969–985.

Cuny, J., P. B. Rhines, P. P. Niiler, and S. Bacon, 2002: Labrador Sea boundary currents and the fate of the Irminger Sea Water. *J. Phys. Oceanogr.,* **32,** 627–647.

Czeschel, L., 2005: The role of eddies for the deep water formation in the Labrador Sea. Ph.D. thesis, Mathematisch-Naturwissenschaftliche Fakultat, Christian-Albrechts-Universitat zu Kiel, 101 pp.

Dengler, M., J. Fisher, F. A. Schott, and R. Zantopp, 2006: Deep Labrador Current and its variability in 1996–2005. *Geophys. Res. Lett.,* **33,** L21S06, doi:101029:2006GL026702.

Dewar, W. K., and C. Gailliard, 1994: The dynamics of barotropically dominated rings. *J. Phys. Oceanogr.,* **24,** 5–29.

Eden, C., and C. Böning, 2002: Sources of eddy kinetic energy in the Labrador Sea. *J. Phys. Oceanogr.,* **32,** 3346–3363.

Hátún, H., A. B. Sandø, H. Drange, B. Hansen, and H. Valdimarsson, 2005: Influence of the Atlantic subpolar gyre on the thermocline circulation. *Science,* **309,** 1841–1844.

——, C. Eriksen, P. B. Rhines, and J. Lilly, 2007: Buoyant eddies entering the Labrador Sea observed with gliders and altimetry. *J. Phys. Oceanogr.,* **37,** 2838–2854.

Heywood, K. J., E. L. McDonagh, and M. A. White, 1994: Eddy kinetic energy of the North Atlantic subpolar gyre from satellite altimetry. *J. Geophys. Res.,* **99,** 22 525–22 539.

Jacob, J. P., E. P. Chassignet, and W. K. Dewar, 2002: Influence of topography on the propagation of isolated eddies. *J. Phys. Oceanogr.,* **32,** 2848–2869.

Katsman, C. A., M. A. Spall, and R. S. Pickart, 2004: Boundary current eddies and their role in the restratification of the Labrador Sea. *J. Phys. Oceanogr.,* **34,** 1967–1983.

LaCasce, J. H., 1998: A geostrophic vortex on a slope. *J. Phys. Oceanogr.,* **28,** 2362–2381.

Lilly, J. M., P. B. Rhines, F. Schott, K. Lavender, J. Lazier, U. Send, and E. D'Asaro, 2003: Observations of the Labrador Sea eddy field. *Prog. Oceanogr.,* **59,** 75–176.

McWilliams, J. C., and G. R. Flierl, 1979: On the evolution of isolated, nonlinear vortices. *J. Phys. Oceanogr.,* **9,** 1155–1182.

Pedlosky, J., 1987: *Geophysical Fluid Dynamics*. 2nd ed. Springer-Verlag, 710 pp.

Pickart, R. S., and M. A. Spall, 2007: Impact of Labrador Sea convection on the North Atlantic meridional overturning circulation. *J. Phys. Oceanogr.,* **37,** 2207–2227.

Prater, M. D., 2002: Eddies in the Labrador Sea as observed by profiling RAFOS floats and remote sensing. *J. Phys. Oceanogr.,* **32,** 411–427.

Samelson, R. M., and J. Pedlosky, 1990: Local baroclinic instability of flow over variable topography. *J. Fluid Mech.,* **221,** 411–436.

Sathiyamoorthy, S., and G. W. K. Moore, 2002: Buoyancy flux at Ocean Weather Station Bravo. *J. Phys. Oceanogr.,* **32,** 458–474.

Spall, M. A., 2004: Boundary current and water mass transformation in marginal seas. *J. Phys. Oceanogr.,* **34,** 1197–1213.

Whitehead, J. A., M. E. Stern, G. R. Flierl, and B. A. Klinger, 1990: Experimental observations of baroclinic eddies on a sloping bottom. *J. Geophys. Res.,* **95,** 9585–9610.

Wolfe, C. L., and C. Cenedese, 2006: Laboratory experiments of eddy generation by a buoyant coastal current flowing over variable bathymetry. *J. Phys. Oceanogr.,* **36,** 395–411.